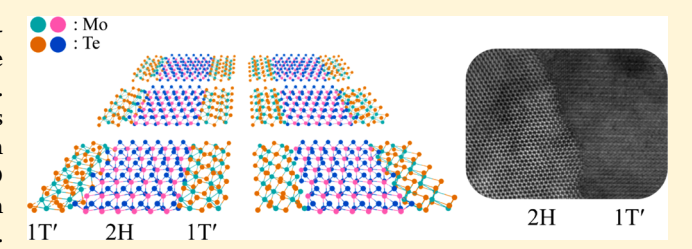
Scaling-up Atomically Thin Coplanar Semiconductor—Metal Circuitry via Phase Engineered Chemical Assembly

Xiaolong Xu,^{†,‡} Shuai Liu,[†] Bo Han,[§] Yimo Han,[∥] Kai Yuan,[†] Wanjin Xu,[†] Xiaohan Yao,[†] Pan Li,[†] Shiqi Yang,[⊥] Wenting Gong,[†] David A. Muller,^{∥,#} Peng Gao,^{‡,§,∇} Yu Ye,*,^{†,‡,○} and Lun Dai*,^{†,‡}

Supporting Information

Downloaded via CORNELL UNIV on April 2, 2020 at 16:30:15 (UTC). See https://pubs.acs.org/sharingguidelines for options on how to legitimately share published articles.

ABSTRACT: Two-dimensional (2D) layered semiconductors, with their ultimate atomic thickness, have shown promise to scale down transistors for modern integrated circuitry. However, the electrical contacts that connect these materials with external bulky metals are usually unsatisfactory, which limits the transistor performance. Recently, contacting 2D semiconductors using coplanar 2D conductors has shown promise in reducing the problematic high contact resistance. However, many of these methods are not ideal for scaled



production. Here, we report on the large-scale, spatially controlled chemical assembly of the integrated 2H-MoTe₂ field-effect transistors (FETs) with coplanar metallic 1T'-MoTe₂ contacts via phase engineered approaches. We demonstrate that the heterophase FETs exhibit ohmic contact behavior with low contact resistance, resulting from the coplanar seamless contact between 2H and 1T'-MoTe₂ confirmed by transmission electron microscopy characterizations. The average mobility of the heterophase FETs was measured to be as high as 23 cm² V⁻¹ s⁻¹ (comparable with those of exfoliated single crystals), due to the large 2H-MoTe₂ single-crystalline domain size ($486 \pm 187 \,\mu\mathrm{m}$). By developing a patterned growth method, we realize the 1T'-MoTe₂ gated heterophase FET array whose components of the channel, gate, and contacts are all 2D materials. Finally, we transfer the heterophase device array onto a flexible substrate and demonstrate the near-infrared photoresponse with high photoresponsivity (~1.02 A/W). Our study provides a basis for the large-scale application of phase-engineered coplanar MoTe₂ semiconductor-metal structure in advanced electronics and optoelectronics.

KEYWORDS: MoTe₂, phase engineering, large-scale, coplanar heterostructure, contact resistance

I ntegrated two-dimensional (2D) electronic circuits based on 2D layered semiconductors, including the transitionmetal dichalcogenides (TMDCs) as well as other 2D semiconductors, such as atomically thin black phosphorus and InSe, etc., promise advanced electronics and flexible devices with increased functionality, performance, and scaling in integrated circuits. $^{1-7}$ The electronic and optoelectronic devices performance is significantly affected by the characteristics of the electrical contacts that connect the semiconductor materials with external circuitry.^{8,9} As the pristine surface of a 2D material has no dangling bonds, it is difficult to form strong interface bonds with metal, thereby increasing the contact resistance.8 Moreover, direct metal electrode deposition on the 2D semiconductor surface causes considerable defects, strain,

disorder, and metal diffusion, resulting in a glassy layer dominated by interdiffusion and strain. 10 Previous efforts, e.g., aligning the metal work function with the conduction/valence band edge of 2D layered semiconductors, showed unsatisfactory high-resistance contacts, due to Fermi level pinning. The traditional method to reduce the contact resistance for silicon is to decrease the depletion region width by locally doping near the silicon-metal junction. However, the 3D doping method used in silicon technology cannot be employed in 2D devices. Recently, contacting 2D semiconductors using

Received: May 16, 2019 Revised: August 17, 2019 Published: September 3, 2019

[†]State Key Laboratory for Artificial Microstructure &Mesoscopic Physics, School of Physics, Peking University, Beijing 100871,

[‡]Collaborative Innovation Center of Quantum Matter, Beijing 100871, China

[§]Electron Microscopy Laboratory, School of Physics, Peking University, Beijing 100871, China

School of Applied and Engineering Physics, Cornell University, Ithaca, New York 14850, United States

¹Academy for Advanced Interdisciplinary Studies, Peking University, Beijing 100871, China

^{*}Kavli Institute at Cornell for Nanoscale Science, Cornell University, Ithaca, New York 14850, United States

VInternational Center for Quantum Materials, School of Physics, Peking University, Beijing 100871, China

CFrontiers Science Center for Nano-optoelectronics, Peking University, Beijing 100871, China

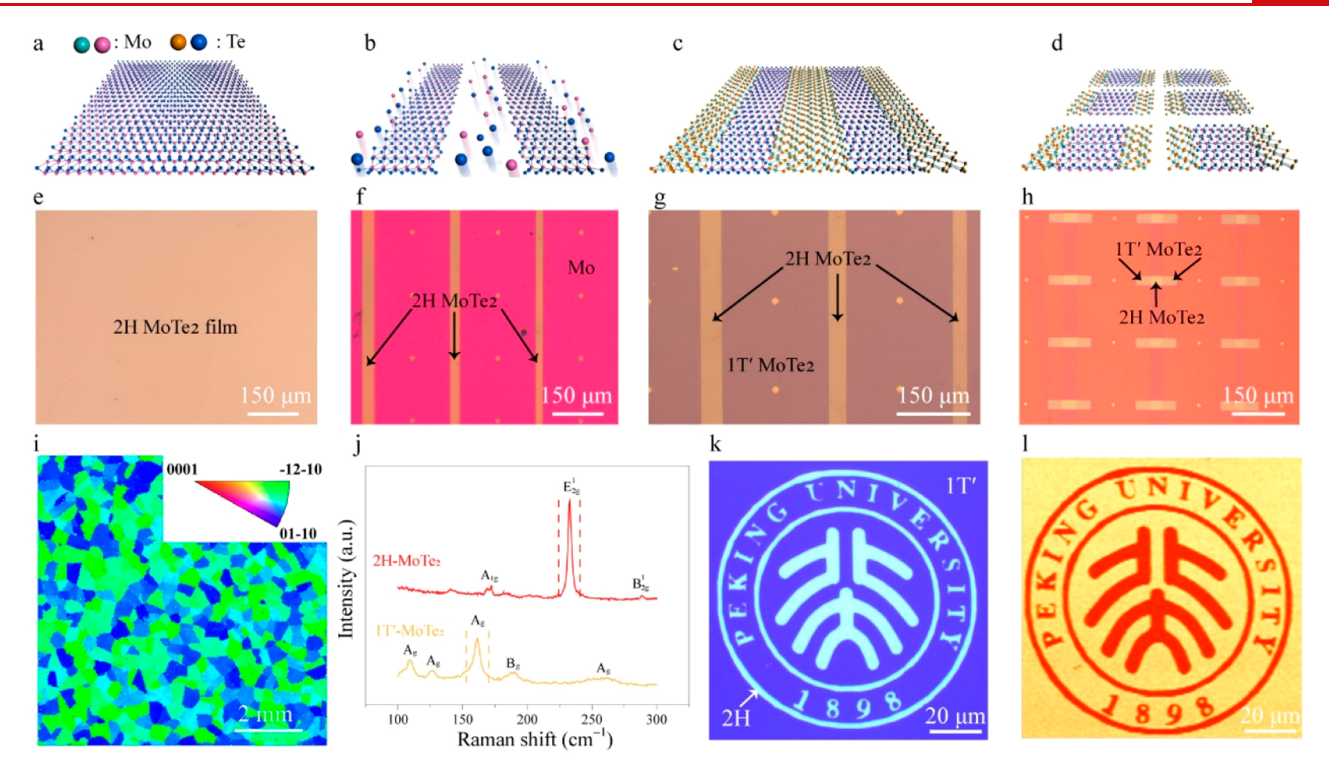


Figure 1. Fabrication processes and Raman characterizations of the 2H/1T' heterophase $MoTe_2$ coplanar structure. (a—h) Schematic illustrations and corresponding optical images of the chemical assembly processes of 2H/1T' heterophase $MoTe_2$. (a,e) High-quality large-scale $2H-MoTe_2$ film was first synthesized on a p^+ -Si/SiO $_2$ substrate via the CVD method. (b,f) $2H-MoTe_2/Mo$ striped patterns were fabricated by photolithography, RIE, and magnetron sputtering Mo, followed by a lift-off process. (c,g) $2H/1T'-MoTe_2$ striped pattern was obtained by a second CVD growth at a lower temperature (530 °C) for 30 min. (d,h) This heterophase structure was patterned into the $1T'/2H/1T'-MoTe_2$ array by photolithography and RIE process. (i) A large-scale EBSD map of the as-synthesized $2H-MoTe_2$ thin film, indicating an average single-crystalline domain size up to $486 \pm 187 \ \mu m$ in the in-plane direction. (j) Raman spectra of the heterophase $MoTe_2$ structure. The Raman spectrum of $2H-MoTe_2$ remains unchanged after the second CVD growth. The well-resolved Raman signatures of $1T'-MoTe_2$ confirm that the Mo thin film was fully tellurized into $1T'-MoTe_2$. (k) Optical image of the PKU logo of the $2H/1T'-MoTe_2$ heterophase structure. (l) Raman spectroscopy mapping of E_{2g}^1 mode of $2H-MoTe_2$ and A_g mode of the $1T'-MoTe_2$. Both the $2H-MoTe_2$ PKU logo and $1T'-MoTe_2$ background are uniform with distinct interfaces.

coplanar 2D conductors has shown promise in reducing the problematic high contact resistance. Reduced contact resistances were observed in metallic 1T-MoS₂/semiconducting 2H-MoS₂, metallic 1T'-MoTe₂/semiconducting 2H-MoTe₂, and metallic VS₂/semiconducting 2H-MoS₂ with seamless coplanar interfaces, which were fabricated using intercalation, laser heating induced phase transition, and heteroepitaxy growth, respectively. However, many of these methods are not ideal for scaled production. The fabrication of these coplanar contacts required the solution processing, suffering from the substitution of chalcogen atoms, or resulted in random place and orientation. It is imperative for practical 2D applications that a scalable (i.e., compatible with wafer-scale technology) method of spatially controlling the semiconductor and metal coplanar interface is realized. Previous studies revealed that MoTe₂ is particularly interesting for phase-engineering applications, as the free energy difference between semiconducting 2H-MoTe₂ and metallic 1T'-MoTe₂ is much smaller (~35 meV per MoTe₂ formula unit) compared with those of other TMDC materials. 18-21 This small energy difference leads to the possibility of phase-controlled synthesis in a large scale.

Here, we demonstrate the large-scale, spatially controlled chemical assembly of 2H-MoTe₂ field-effect transistors (FETs) integrated with coplanar metallic 1T′-MoTe₂ contacts via phase engineering. The heterophase FETs exhibit ohmic contact behavior with a low contact resistance of \sim 1.1 k Ω

 μ m at a high doping level and high average carrier mobility of $\sim\!23~{\rm cm}^2~{\rm V}^{-1}~{\rm s}^{-1}$. We also developed a patterned growth method of $1{\rm T'}$ -MoTe $_2$ and realized $1{\rm T'}$ -MoTe $_2$ gated heterophase FET arrays whose components of channel, gate, and contacts are all 2D materials. Each FET has an independently patterned $1{\rm T'}$ -MoTe $_2$ gate electrode, which is required for logic circuitry. Few-layer 2H-MoTe $_2$, with a bandgap of $\sim\!1$ eV, is a candidate material for near-infrared (NIR) photodetector. $^{15-17}$ We transferred the heterophase device onto a flexible substrate and demonstrated the NIR photoresponse with enhanced photoresponsivity ($\sim\!1.02~{\rm A/W}$) due to the reduced contact resistance. Our study shows the promise of large-scale applications using a 2D coplanar heterophase structure for advanced electronic and optoelectronic devices.

Results and Discussion. Patterned Chemical Assembly of the Heterophase MoTe₂ on a Large Scale. To chemically assemble large-scale coplanar 2H-1T' heterophase MoTe₂, a high-quality few-layer 2H-MoTe₂ film was first synthesized on a p^+ -Si/SiO₂ substrate via chemical vapor deposition (CVD) (Figure 1a). Our previous work has found the synthesis of 2H-MoTe₂ film was driven by the solid-to-solid 1T' to 2H-MoTe₂ phase transformation, ²² which can be well described by the time—temperature—transformation diagram. First, a 1–1.5 nm thick Mo film was prepared on the Si/SiO₂ substrate via magnetron sputtering. Then, the MoTe₂ films were grown by tellurizing the Mo film at 650 °C for 2 h. During the

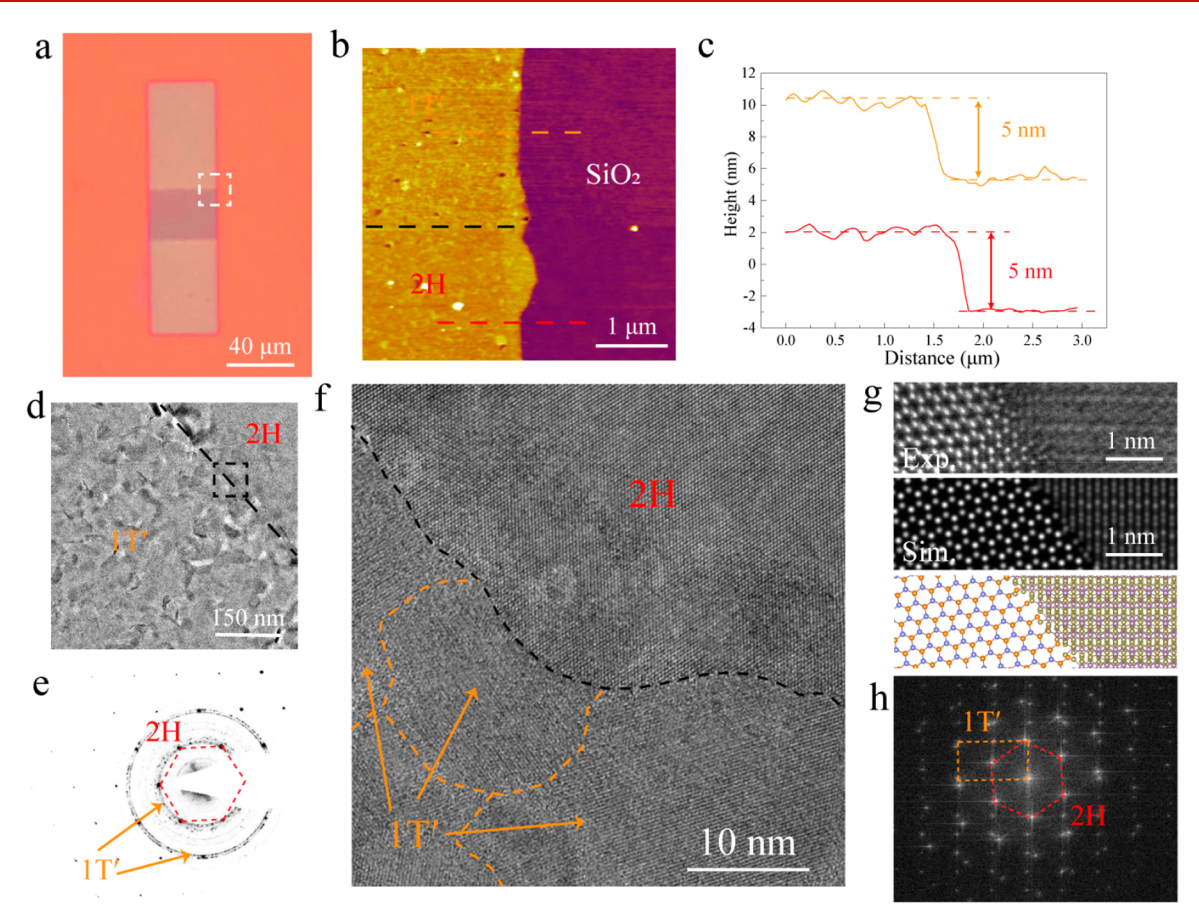


Figure 2. AFM and HR-TEM characterizations of the 2H/1T′-MoTe₂ interface. (a) Optical image of a 1T′/2H/1T′ heterophase MoTe₂ structure. The interface area (labeled by the dashed box) was measured by the AFM. (b) AFM height image at the 2H/1T′-MoTe₂ interface. The nearly homogeneous color contrast indicates the uniformity of the sample thickness at the 2H and 1T′-MoTe₂ regions. (c) Height line profiles at 2H-MoTe₂ and 1T′-MoTe₂ regions, respectively, showing an identical thickness of about 5 nm. (d) Large field-of-view TEM image at the 2H/1T′-MoTe₂ interface. (e) SAED pattern at the interface, which comprised a single set of diffraction spots with 6-fold symmetry related to the single-crystalline 2H-MoTe₂ and a series of diffraction rings related to the polycrystalline 1T′-MoTe₂. (f) HR-TEM image at the interface. 1T′-MoTe₂ domains with a size of about tens of nanometer stitched seamlessly to 2H-MoTe₂ with random orientations. (g) Experimental and simulated HAADF-STEM images as well as the schematic lattices of a representative 1T′/2H-MoTe₂ interface, showing atomically smooth interface and seamless contact. (h) Corresponding FFT pattern of the experimental HAADF-STEM image, showing a set of monoclinic 1T′ diffraction spots and a set of hexagonal 2H diffraction spots.

tellurization, 1T' phase polycrystalline MoTe₂ film with Te vacancies was first synthesized. As Te atoms occupy the vacancies in the 1T' phase film, the phase transformation from 1T' to 2H-MoTe₂ occurs and diffuses into circles, where the recrystallization occurs at the boundary of 1T'-MoTe2 and 2H-MoTe₂. As growth time prolongs, all the circles merge and become a uniform 2H phase MoTe₂ film. By controlling the kinetic rates of nucleation and crystal growth, we were able to synthesize large-scale continuous 1T'-MoTe₂ and 2H-MoTe₂ thin films, as well as arbitrary shaped 1T'-MoTe₂ (see Supplementary Section Ia). This method allowed us to also synthesize a centimeter-scale 2H-MoTe2 thin film with a domain size up to several hundred micrometers under 650 °C for 2 h (Figure 1e) (see details in Methods). The large-scale electron backscatter diffraction (EBSD) map of the assynthesized 2H-MoTe₂ thin film shows a uniform contrast in the out-of-plane direction (see Supplementary Section Ib), indicating that the highly textured MoTe₂ thin film was stacked in the c-axis, with an average domain size up to 486 \pm 187 μ m in the in-plane direction (Figure 1i). The domain size (d) is calculated based on a circularly equivalent area $(d = \sqrt{4s/\pi})$, where s is the statistically averaged domain area. The regular Hall bar structure was fabricated to measure the intrinsic carrier mobility of the synthesized 2H-MoTe₂ (see Supplementary Section Ic). The Hall mobility $\mu_{\rm H}$ is extracted to be 95 cm² V⁻¹ s⁻¹ at room temperature, indicating the high quality of the 2H-MoTe₂. The large-scale 2H-MoTe₂ film Hall mobility was also measured via a van Der Pauw method (see Supplementary Section Ic). The hall mobility $\mu_{\rm H}$ is extracted to be 31 cm² V⁻¹ s⁻¹, which is lower than that measured by regular Hall bar structure. This is because of the existence of the grain boundaries in the large-scale film, which scatter the carriers and reduce the mobility.

Following the growth, large-scale 2H-MoTe₂/Mo is fabricated into stripes using photolithography, reactive ion etching (RIE), and magnetron sputtering (Mo deposition), followed by a lift-off process (Figure 1b,f). Subsequently, the sample was sent back into the furnace at a lower temperature (530 °C) for 30 min. After the second CVD growth, the Mo film was tellurized to 1T′-MoTe₂, while the 2H-MoTe₂ remained unaffected (see Supplementary Section Id). Ultimately, this formed striped patterns of 2H/1T′-MoTe₂ (Figure 1c,g). This was confirmed by the appearance of the well-resolved A_g Raman modes (107, 127, 161, and 256 cm⁻¹)

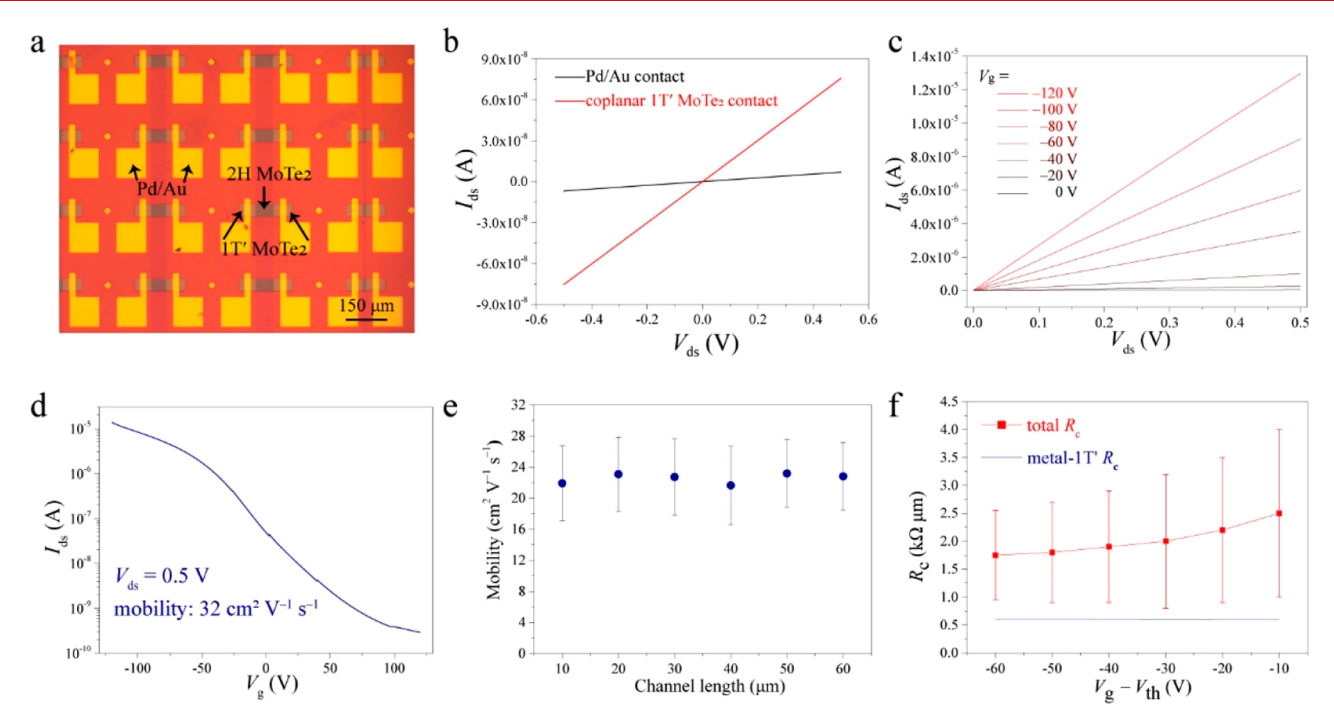


Figure 3. Room-temperature electrical properties of the 2H/1T'-MoTe₂ coplanar heterophase FETs. (a) Optical image of the heterophase FET device array with different channel lengths. (b) $I_{\rm ds}-V_{\rm ds}$ curves of a representative coplanar 1T'-MoTe₂ contacted and direct Pd/Au metal contacted 2H-MoTe₂ channel under zero back gate voltage. The coplanar 1T'-MoTe₂ contact showed superior contact. (c) Typical $I_{\rm ds}-V_{\rm ds}$ curves of the heterophase FET measured under various gate voltages. All the $I_{\rm ds}-V_{\rm ds}$ curves exhibited linear ohmic contact behavior. (d) Corresponding transfer curve of the heterophase FET, showing *p*-type channel characteristics with an on-off ratio of ~1 × 10⁴. The room-temperature field-effect mobility was estimated to be ~32 cm² V⁻¹ s⁻¹. (e) Field-effect mobilities for different channel length measured on 100 devices. All the mobilities hover in a range of 20–24 cm² V⁻¹ s⁻¹ and are independent of the channel length, due to the large single-crystalline domain of the 2H-MoTe₂. (f) Contact resistance of the heterophase and 1T'-MoTe₂ only devices extracted using the transfer length method. The total contact resistance shows strong gate dependence, while the contact resistance of 1T'-MoTe₂ is about 0.6 kΩ μm, independent of the gate voltage. The measured minimum value of the total contact resistance is about ~1.7 kΩ μm, which was obtained at high doping, yielding a coplanar 1T'/2H-MoTe₂ contact resistance of ~1.1 kΩ μm.

of 1T'-MoTe₂ and the out-of-plane A_{1g} (171 cm⁻¹), B_{2g}^1 (291 cm⁻¹), and the strong in-plane E_{2g} (234 cm⁻¹) Raman modes of 2H-MoTe₂ in the respective regions (Figure 1j). This heterophase pattern was further fabricated into isolated 1T'/2H/1T'-MoTe₂ arrays by photolithography and reactive ion etching (RIE, Figure 1d,h). Using electron beam lithography (EBL) in place of photolithography, we also synthesized arbitrarily controlled coplanar 2H/1T'-MoTe₂ heterophase structures with smaller feature sizes, e.g., Peking University's (PKU) logo (Figure 1k). Raman spectroscopy mapping of the representative 2H-MoTe₂ E_{2g} mode and 1T'-MoTe₂ A_{g} mode (labeled by the corresponding dashed lines in Figure 1j) clearly shows that both the 2H-MoTe₂ PKU logo and 1T'-MoTe₂ background are uniform, with clear and distinct interfaces (Figure 1l).

Characterizations of the Interface of the Coplanar 2H/1T' Heterophase MoTe₂. The interface between 2H-MoTe₂ and 1T'-MoTe₂ was characterized using atomic force microscopy (AFM), the Kelvin probe force microscopy (KPFM) and transmission electron microscopy (TEM). The typical optical image of an isolated 1T'/2H/1T'-MoTe₂ coplanar heterostructure showed a large contrast difference between respective regions (Figure 2a), resulting from the significant dielectric constant difference between the semiconducting 2H-MoTe₂ and metallic 1T'-MoTe₂. The AFM height image at the 2H/1T'-MoTe₂ interface (Figure 2b) exhibited a nearly homogeneous color contrast, indicating the uniformity of the sample thickness. The line profiles of the 2H-MoTe₂ and 1T'-MoTe₂

(Figure 2c) regions showed a similar thickness of about 5 nm (corresponding to 7-layer $MoTe_2$), ²⁴ resulting from the precise control of the Mo film thickness. Additionally, the line profile across the interface (see Supplementary Section IIa) did not show any stitches or flake overlaps, confirming the seamless coplanar contact between the heterophase.

The surface work function image measured by KPFM and the potential line profile (see Supplementary Section IIb) show a sharp demarcation between the 1T'-MoTe2 and 2H-MoTe2, with a potential difference between them of ~27.5 mV. Notably, the measured higher work function of the 1T'-MoTe₂ is preferable for the ohmic contact of the p-type 2H-MoTe₂. To evaluate the crystallinity of the heterophase, we transferred 1T'/2H/1T'-MoTe₂ arrays onto a copper grid (see Supplementary Section IIIa). At the interface of 2H/1T'-MoTe₂ (Figure 2d), the selected area electron diffraction (SAED) pattern (Figure 2e) comprised a single set of diffraction spots with 6-fold symmetry related to the single-crystalline 2H-MoTe₂ together with a series of diffraction rings related to the polycrystalline 1T'-MoTe₂.²⁵ The high-resolution TEM (HR-TEM) image (Figure 2f) showed the interface contains polycrystalline monoclinic (1T') structure domains of about tens of nanometers and a single hexagonal (2H) structure domain. We further used high-angle annular dark-field scanning TEM (HAADF-STEM) to resolve in-plane atomic arrangements of a typical 1T'/2H-MoTe₂ interface (Figure 2g), where an atomically smooth interface transition was observed. The corresponding FFT pattern contained a set of

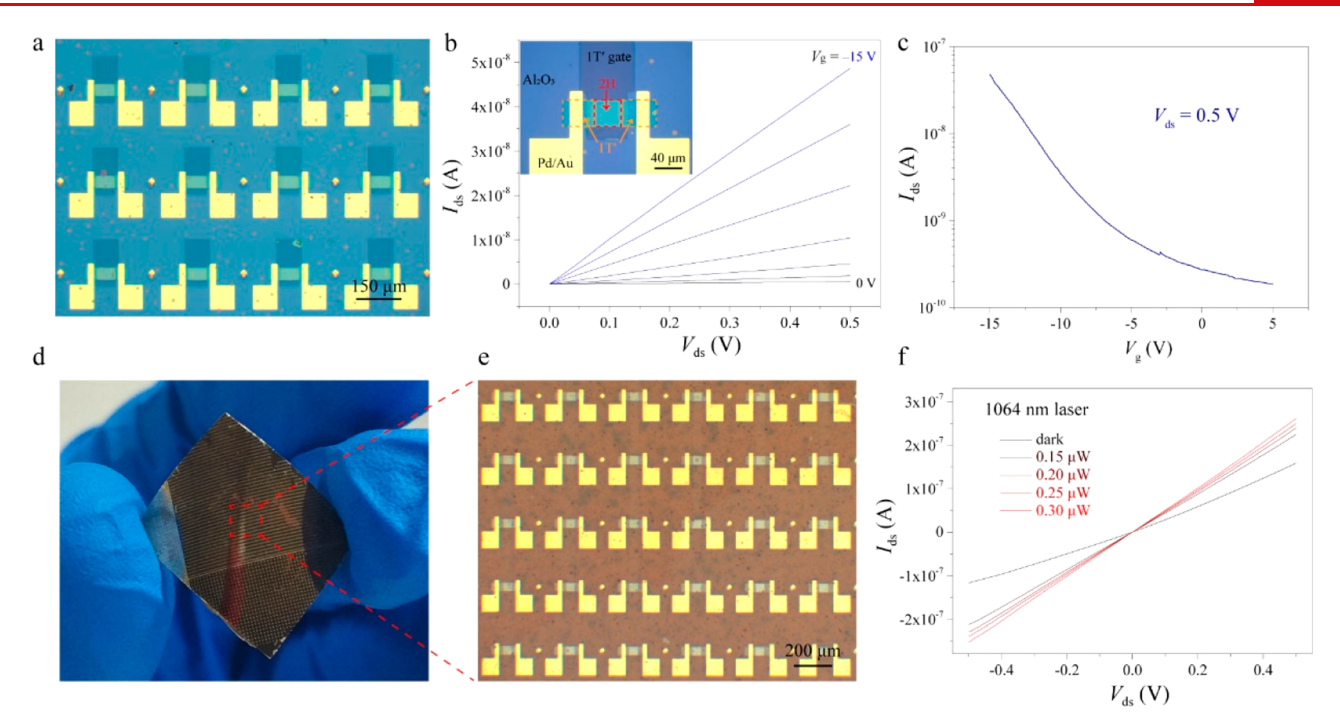


Figure 4. 1T'-MoTe $_2$ gated heterophase transistor and the flexible NIR photodetector. (a) Optical image of the 1T'-MoTe $_2$ gated heterophase FET array. The 1T'-MoTe $_2$ local gate electrodes were fabricated via the patterned growth method. (b) Typical I_{ds} - V_{ds} curves of a 1T'-MoTe $_2$ gated heterophase FET measured under various gate voltages. All the I_{ds} - V_{ds} curves exhibited linear ohmic contact behavior. Inset: the zoomed-in optical image of the 1T'-MoTe $_2$ gated heterophase FET device. (c) Transfer curve of the 1T'-MoTe $_2$ gated heterophase FET, showing a p-type characteristic. (d,e) Photograph and optical image of the transferred 1T'/2H/1T'-MoTe $_2$ heterophase devices on a flexible polyimide substrate. The heterostructure maintained its integrity on a large scale after being transferred. (f) I-V curves of the heterophase photodetector under 1064 nm laser illumination with different incident light powers, showing obvious NIR photoresponse.

monoclinic 1T' spots and a set of hexagonal 2H spots (Figure 2h). The simulated HAADF-STEM image, as well as the schematic lattices (Figure 2g) at the interface, is provided, which agree well with the observed results. We found the 1T' domains stitched seamlessly to single-crystalline 2H-MoTe $_2$ with random orientations at different locations of the interface (see Supplementary Section IIIb).

Electrical Properties of the Coplanar Heterophase MoTe₂ FETs. The seamless contact allowed us to inject current into semiconducting 2H-MoTe₂ from metallic 1T'-MoTe₂ electrodes with reduced contact resistance (R_c) . By using coplanar seamless contacts, the reduced contact resistance is of great significance to the development of practical 2D semiconductor applications. The large-scale coplanar heterophase MoTe₂ FETs array with different channel lengths was fabricated (Figure 3a). Pd/Au electrodes (10/50 nm) were deposited on the 1T' parts of each 1T'/2H/1T'-MoTe₂ structure for electrical measurements. The p^+ -Si was used as the back gate electrode. The devices array with Pd/Au electrodes directly deposited on the 2H phase were fabricated for comparison (see Supplementary Section IVa). With the same channel length, the current injected from coplanar 1T'-MoTe₂ contact was 1 order of magnitude larger than that from the deposited Pd/Au metal contact (Figure 3b), indicative of lower contact resistance at the 1T'/2H-MoTe₂ interface. The typical sourcedrain current (I_{ds}) versus source-drain voltage (V_{ds}) curves measured at various gate voltages (Figure 3c) showed linear behavior, confirming the ohmic contact between the 1T' and 2H-MoTe₂. The gate voltage (V_g) dependence of the heterophase FET under a bias voltage of 0.5 V showed ptype channel characteristics with an on-off ratio of $\sim 1 \times 10^4$ (Figure 3d). The room-temperature field-effect mobility (μ)

was ~32 cm² V⁻¹ s⁻¹, using $\mu = (\mathrm{d}I_{\mathrm{ds}}/\mathrm{d}V_{\mathrm{g}})$ (L/W) ($1/V_{\mathrm{ds}}C_{\mathrm{g}}$), where L, W, and C_{g} are the channel length, channel width, and the gate capacitance per unit area, respectively. By contrast, the field-effect mobilities extracted from Pd/Au contacted 2H-MoTe₂ FETs are only 2 cm² V⁻¹ s⁻¹ (see Supplementary Section IVa). We measured 100 FETs with different change lengths and found that the average mobility (in a range of 20–24 cm² V⁻¹ s⁻¹, comparable to the reported values for exfoliated 2H-MoTe₂ single crystals) ^{12,13} was independent of the channel length (Figure 3e). This was not surprising, as our average 2H-MoTe₂ single-crystalline domain size (~486 μ m) was much larger than the largest channel length (60 μ m) being measured. Hence, there were unlikely to be many grain boundaries that could act as scattering centers.

To determine the contact resistance between the 1T'-MoTe₂ and 2H-MoTe₂, we used the transfer length method (TLM),9 in which the channel length-dependent resistances of both the 1T'/2H/1T' coplanar heterophase structure (see Supplementary Section IVb) and 1T'-MoTe₂ (see Supplementary Section IVc) were measured. The total R_c of the metal/1T'/2H-MoTe₂ structure contains the R_c of metal/1T'- $MoTe_2$ and the R_c of $1T'/2H-MoTe_2$. The total R_c (metal/ 1T'/2H-MoTe₂) shows a strong dependence on the back gate voltage due to the semiconducting nature of 2H-MoTe₂. In contrast, due to the metallic nature of 1T'-MoTe₂, the R_c of metal/1T'-MoTe₂ was observed at a constant of \sim 0.6 k Ω μ m, independent of the back gate voltage (Figure 3f). The minimum total R_c was measured to be ~1.7 k Ω μ m at a higher turn-on gate voltage (Figure 3f). Thus, the corresponding R_c at the 1T'/2H-MoTe₂ interface is ~1.1 k Ω μ m, which is about 2 orders of magnitude smaller than those of metalcontacted 2H-MoTe₂ (reported value of 409 k Ω μ m).

1T'-MoTe₂ Gated Heterophase Transistor and NIR Flexible Photodetector. To realize 2D circuitry, it is required to control each transistor independently. Technical challenges and future trends are presented for the application of transparent electrodes in flexible electronics. Here, we chemically assembled the coplanar 1T'/2H/1T'-MoTe₂ array on top of the prepatterned 1T'-MoTe₂ gate electrodes (Figure 4a). The 1T'-MoTe₂ patterns were synthesized via the developed patterned growth method (see Supplementary Section Ia). A layer of 30 nm Al₂O₃ (via atomic layer deposition (ALD)) was used as the gate dielectric. The detailed fabrication process is provided in the Methods and Supplementary Section IVd. For a typical 1T'-MoTe₂ gated heterophase transistor (inset of Figure 4b), the I-V curves measured at various gate voltages showed linear behavior (Figure 4b), indicating the ohmic contact between the coplanar 1T'/2H-MoTe₂. The transfer curve exhibited a clear p-type channel characteristic as well (Figure 4c). Compared with the device depicted in Figure 3a, the oncurrent of the transistor is about 1 order of magnitude lower, possibly due to n-type doping effect induced by the ALD Al₂O₃ (see Supplementary Section IVe).²⁶ It is reasonable to envision that the device performance can be further improved by replacing Al_2O_3 with hBN.

With a bandgap of ~1.0 eV, few-layer 2H-MoTe₂ can be used for near-infrared (NIR) photodetection.¹⁷ Due to the reduced contact resistance of our device scheme, it is reasonable to assume improved photodetection performance over a large scale. To fabricate these photodetectors, we transferred the large-scale 1T'/2H/1T'-MoTe2 array to a flexible polyimide (PI) substrate (Figure 4d, see Methods for details). The heterostructure maintains its integrity on a large scale after the transfer (Figure 4e). We investigated the photoresponse behavior of the heterophase under 1064 nm laser illumination with various incident light powers, where we found the photocurrent increased with increasing incident light power (Figure 4f). It is worth noting that when the incident 1064 nm laser power is 50 nW, the photoresponsivity ($R = \Delta I/$ *P*, where ΔI is the difference between the photocurrent and the dark current and P is the incident light power illuminated on the sample) was as high as 1.02 A/W at $V_{ds} = 0.5$ V. The photoresponsivity deceased with increased incident light power (see Supplementary Section V), possibly due to the reduction of the number of carriers that could be collected under high photon flux.²⁹ Thus, the coplanar 1T'/2H/1T' heterophase can be a promising candidate for future NIR flexible and transparent optoelectronics.

Conclusion. We demonstrated spatially controlled chemical assembly of integrated 1T'/2H/1T' coplanar heterophase MoTe₂ FETs across a centimeter-scale via phase engineered growth. Such coplanar interfaces are atomically sharp and seamless across the two phases. This approach established a new type of atomic-scale electrical contact. The heterophase contact FETs exhibited ohmic contact with reduced contact resistance. We observed that the field-effect mobility of the 2H-MoTe₂ can rival that of the exfoliated single crystalline samples, due to the large domain size (up to 486 μ m) of the as-synthesized 2H-MoTe₂. With the developed spatialcontrolled patterned growth method, we fabricated 1T'-MoTe₂ gated heterophase FET arrays, whose components of the channel, gate, and contact electrodes are all 2D materials. We also transferred the heterophase device array onto a flexible substrate and demonstrated NIR photoresponse with high

photoresponsivity. Our spatial-controlled large-scale chemical assembly of coplanar conductor-semiconductor heterophase structure provides a route toward industry compatible wafer-scale high-performance 2D electronics and optoelectronics.

Methods. Synthesis of the 2H and 1T'-MoTe₂ Films. The MoTe₂ films were synthesized by tellurizing the Mo films at atmospheric pressure using a horizontal tube furnace equipped with mass flow controllers and a vacuum pump. Mo films were deposited on Si/SiO2 substrates using magnetron sputtering. The substrates and Te powders were placed in an alumina boat, which was later inserted into a one-inch diameter quartz tube inside the furnace. After evacuating the quartz tube to less than 10 mTorr, high purity Ar gas started to flow at a rate of 500 standard cubic centimeter per minute (sccm) until atmospheric pressure was reached. After that, Ar and H₂ flowed at rates of 4 and 5 sccm, respectively. The furnace was ramped to 650 °C for 2 h and 530 °C for 30 min to synthesize 2H and 1T'-MoTe2 films, respectively. After growth, the furnace was cooled down to room temperature naturally. For the patterned growth of MoTe2, Mo film was prepatterned by either photolithography or EBL followed by magnetron sputtering and lift-off process.

Transfer of the 1T'/2H/1T' Heterophase MoTe₂ Array. The heterophase MoTe₂ array on the Si/SiO₂ substrate was spin-coated with a poly methyl methacrylate (PMMA) layer under 3000 rpm for 60 s. After being baked at 100 °C for 2 min, the sample was immersed in a dilute HF solution (1.5%) at room temperature for 10 min. Subsequently, the heterophase MoTe₂ array with PMMA was gently peeled off from Si/SiO₂ substrate in deionized water and transferred onto a mesh copper grid with carbon film on top for TEM characterization or a PI substrate for flexible device investigation. Finally, the PMMA was removed using acetone, and the sample was thoroughly rinsed with isopropyl alcohol (IPA).

Fabrication of the 1T'-MoTe $_2$ Gated Heterophase Transistors. First, the bottom 1T'-MoTe $_2$ gate electrodes were grown by the patterned growth method on the p^+ -Si/SiO $_2$ (285 nm) substrate. Second, a layer of 30 nm Al $_2$ O $_3$ was deposited by atomic layer deposition (ALD). Next, a pregrown 2H-MoTe $_2$ film was transferred onto the Al $_2$ O $_3$ layer by the above-described transfer method (see Methods for details). Finally, the 1T'/2H/1T'-MoTe $_2$ heterophase structures were obtained by the phase engineered chemical assembly method described in the main text. Spatial-controlled photolithography is needed to define the 2H-MoTe $_2$ channels on top of the 1T' MoTe $_2$ gate electrodes. For the convenience of measurement, 10/50 nm Pd/Au metal electrodes were fabricated to contact the 1T'-MoTe $_2$.

ASSOCIATED CONTENT

Supporting Information

The Supporting Information is available free of charge on the ACS Publications website at DOI: 10.1021/acs.nanolett.9b02006.

Patterned growth of 1T'-MoTe₂; Hall measurements of the 2H-MoTe₂; AFM and KPFM characterizations across the 1T'/2H-MoTe₂ interface; TEM characterizations of the coplanar 1T'/2H-MoTe₂; Pd/Au contacted 2H-MoTe₂ for comparison; the total contact resistance of metal/1T'/2H-MoTe₂; contact resistance between metal and 1T'-MoTe₂; 1T'-MoTe₂ gated heterophase transistor; *n*-type doping induced by the

ALD Al_2O_3 ; power dependence NIR photodetection of the heterophase device (PDF)

AUTHOR INFORMATION

Corresponding Authors

*(Y.Y.) E-mail: ye_yu@pku.edu.cn. *(L.D.) E-mail: lundai@pku.edu.cn.

ORCID ®

Yimo Han: 0000-0003-0563-4611 David A. Muller: 0000-0003-4129-0473 Peng Gao: 0000-0003-0860-5525

Yu Ye: 0000-0001-6046-063X Lun Dai: 0000-0002-6317-6340

Notes

The authors declare no competing financial interest.

ACKNOWLEDGMENTS

This work was supported by the National Natural Science Foundation of China (Nos. 61874003, 61521004, 11474007, 51672007, 11974023), Nation Key R&D Program of China (Grant Nos. 2018YFA0306900 and 2017YFA0206301), and Beijing Natural Science Foundation (4182028). Y.H. and D.M. were supported by NSF Grant (DMR-1719875). G.P. was supported by Key Area R&D Program of Guangdong Province (2018B010109009), and the Key R&D Program of Guangdong Province (2018B030327001). We acknowledge Electron Microscopy Laboratory in Peking University for the use of Cs corrected electron microscope.

■ REFERENCES

- (1) Lin, Z.; Liu, Y.; Halim, U.; Ding, M.; Liu, Y.; Wang, Y.; Jia, C.; Chen, P.; Duan, X.; Wang, C.; Song, F.; Li, M.; Wan, C.; Huang, Y.; Duan, X. Solution- processable 2D semiconductors for high-performance large-area electronics. *Nature* **2018**, *562* (7726), 254–258.
- (2) Kang, K.; Lee, K.-H.; Han, Y.; Gao, H.; Xie, S.; Muller, D. A.; Park, J. Layer-by-layer assembly of two-dimensional materials into wafer-scale heterostructures. *Nature* **2017**, *550*, 229.
- (3) Yu, H.; Liao, M.; Zhao, W.; Liu, G.; Zhou, X. J.; Wei, Z.; Xu, X.; Liu, K.; Hu, Z.; Deng, K.; Zhou, S.; Shi, J.-A.; Gu, L.; Shen, C.; Zhang, T.; Du, L.; Xie, L.; Zhu, J.; Chen, W.; Yang, R.; Shi, D.; Zhang, G. Wafer-scale growth and transfer of highly-oriented monolayer MoS₂ continuous films. *ACS Nano* **2017**, *11* (12), 12001–12007.
- (4) Xue, Y.; Zhang, Y.; Liu, Y.; Liu, H.; Song, J.; Sophia, J.; Liu, J.; Xu, Z.; Xu, Q.; Wang, Z.; Zheng, J.; Liu, Y.; Li, S.; Bao, Q. Scalable production of a few-layer MoS₂/WS₂ vertical heterojunction array and its application for photodetectors. *ACS Nano* **2016**, *10* (1), 573–580.
- (5) Li, L.; Yang, F.; Ye, G. J.; Zhang, Z.; Zhu, Z.; Lou, W.; Zhou, X.; Li, L.; Watanabe, K.; Taniguchi, T.; Chang, K.; Wang, Y.; Chen, X. H.; Zhang, Y. Quantum Hall effect in black phosphorus two-dimensional electron system. *Nat. Nanotechnol.* **2016**, *11*, 593.
- (6) Bandurin, D. A.; Tyurnina, A. V.; Yu, G. L.; Mishchenko, A.; Zólyomi, V.; Morozov, S. V.; Kumar, R. K.; Gorbachev, R. V.; Kudrynskyi, Z. R.; Pezzini, S.; Kovalyuk, Z. D.; Zeitler, U.; Novoselov, K. S.; Patanè, A.; Eaves, L.; Grigorieva, I. V.; Fal'ko, V. I.; Geim, A. K.; Cao, Y. High electron mobility, quantum Hall effect and anomalous optical response in atomically thin InSe. *Nat. Nanotechnol.* **2017**, *12*, 223.
- (7) Qiu, G.; Wang, Y.; Nie, Y.; Zheng, Y.; Cho, K.; Wu, W.; Ye, P. D. Quantum transport and band structure evolution under high magnetic field in few-layer tellurene. *Nano Lett.* **2018**, *18* (9), 5760–5767.
- (8) Allain, A.; Kang, J.; Banerjee, K.; Kis, A. Electrical contacts to two-dimensional semiconductors. *Nat. Mater.* **2015**, *14*, 1195.

(9) English, C. D.; Shine, G.; Dorgan, V. E.; Saraswat, K. C.; Pop, E. Improved contacts to MoS2 transistors by ultra-high vacuum metal deposition. *Nano Lett.* **2016**, *16* (6), 3824–3830.

- (10) Liu, Y.; Guo, J.; Zhu, E.; Liao, L.; Lee, S.-J.; Ding, M.; Shakir, I.; Gambin, V.; Huang, Y.; Duan, X. Approaching the schottky—mott limit in van der Waals metal—semiconductor junctions. *Nature* **2018**, 557 (7707), 696–700.
- (11) Kappera, R.; Voiry, D.; Yalcin, S. E.; Branch, B.; Gupta, G.; Mohite, A. D.; Chhowalla, M. Phase-engineered low-resistance contacts for ultrathin MoS₂ transistors. *Nat. Mater.* **2014**, *13*, 1128.
- (12) Cho, S.; Kim, S.; Kim, J. H.; Zhao, J.; Seok, J.; Keum, D. H.; Baik, J.; Choe, D.-H.; Chang, K. J.; Suenaga, K.; Kim, S. W.; Lee, Y. H.; Yang, H. Phase patterning for ohmic homojunction contact in MoTe₂. Science **2015**, 349 (6248), 625.
- (13) Sung, J. H.; Heo, H.; Si, S.; Kim, Y. H.; Noh, H. R.; Song, K.; Kim, J.; Lee, C. S.; Seo, S. Y.; Kim, D. H.; Kim, H. K.; Yeom, H. W.; Kim, T. H.; Choi, S. Y.; Kim, J. S.; Jo, M. H. Coplanar semiconductormetal circuitry defined on few-layer MoTe₂ via polymorphic heteroepitaxy. *Nat. Nanotechnol.* **2017**, *12* (11), 1064–1070.
- (14) Leong, W. S.; Ji, Q.; Mao, N.; Han, Y.; Wang, H.; Goodman, A. J.; Vignon, A.; Su, C.; Guo, Y.; Shen, P.-C.; Gao, Z.; Muller, D. A.; Tisdale, W. A.; Kong, J. Synthetic lateral metal-semiconductor heterostructures of transition metal disulfides. *J. Am. Chem. Soc.* **2018**, *140* (39), 12354–12358.
- (15) Duerloo, K.-A. N.; Li, Y.; Reed, E. J. Structural phase transitions in two-dimensional Mo- and W-dichalcogenide monolayers. *Nat. Commun.* **2014**, *5*, 4214.
- (16) Li, Y.; Duerloo, K.-A. N.; Wauson, K.; Reed, E. J. Structural semiconductor-to-semimetal phase transition in two-dimensional materials induced by electrostatic gating. *Nat. Commun.* **2016**, *7*, 10671
- (17) Song, S.; Keum, D. H.; Cho, S.; Perello, D.; Kim, Y.; Lee, Y. H. Room temperature semiconductor—metal transition of MoTe₂ thin films engineered by strain. *Nano Lett.* **2016**, *16* (1), 188–193.
- (18) Keum, D. H.; Cho, S.; Kim, J. H.; Choe, D.-H.; Sung, H.-J.; Kan, M.; Kang, H.; Hwang, J.-Y.; Kim, S. W.; Yang, H.; Chang, K. J.; Lee, Y. H. Bandgap opening in few-layered monoclinic MoTe₂. *Nat. Phys.* **2015**, *11*, 482.
- (19) Octon, T. J.; Nagareddy, V. K.; Russo, S.; Craciun, M. F.; Wright, C. D. Fast high-responsivity few-layer MoTe₂ photodetectors. *Adv. Opt. Mater.* **2016**, *4* (11), 1750–1754.
- (20) Zhang, K.; Fang, X.; Wang, Y.; Wan, Y.; Song, Q.; Zhai, W.; Li, Y.; Ran, G.; Ye, Y.; Dai, L. Ultrasensitive near-infrared photodetectors based on a graphene–MoTe₂–graphene vertical van der Waals heterostructure. ACS Appl. Mater. Interfaces 2017, 9 (6), 5392–5398.
- (21) Bie, Y.-Q.; Grosso, G.; Heuck, M.; Furchi, M. M.; Cao, Y.; Zheng, J.; Bunandar, D.; Navarro-Moratalla, E.; Zhou, L.; Efetov, D. K.; Taniguchi, T.; Watanabe, K.; Kong, J.; Englund, D.; Jarillo-Herrero, P. A MoTe₂-based light-emitting diode and photodetector for silicon photonic integrated circuits. *Nat. Nanotechnol.* **2017**, *12*, 1124.
- (22) Xu, X.; Chen, S.; Liu, S.; Cheng, X.; Xu, W.; Li, P.; Wan, Y.; Yang, S.; Gong, W.; Yuan, K.; Gao, P.; Ye, Y.; Dai, L. Millimeter-scale single-crystalline semiconducting MoTe₂ via solid-to-solid phase transformation. *J. Am. Chem. Soc.* **2019**, *141* (5), 2128–2134.
- (23) Blake, P.; Hill, E. W.; Castro Neto, A. H.; Novoselov, K. S.; Jiang, D.; Yang, R.; Booth, T. J.; Geim, A. K. Making graphene visible. *Appl. Phys. Lett.* **2007**, *91* (6), 063124.
- (24) Zhou, L.; Xu, K.; Zubair, A.; Liao, A. D.; Fang, W.; Ouyang, F.; Lee, Y.-H.; Ueno, K.; Saito, R.; Palacios, T.; Kong, J.; Dresselhaus, M. S. Large-area synthesis of high-quality uniform few-layer MoTe₂. *J. Am. Chem. Soc.* **2015**, *137* (37), 11892–11895.
- (25) Yun, S. J.; Han, G. H.; Kim, H.; Duong, D. L.; Shin, B. G.; Zhao, J.; Vu, Q. A.; Lee, J.; Lee, S. M.; Lee, Y. H. Telluriding monolayer MoS₂ and WS₂ via alkali metal scooter. *Nat. Commun.* **2017**, 8 (1), 2163.
- (26) Tang, H.-L.; Chiu, M.-H.; Tseng, C.-C.; Yang, S.-H.; Hou, K.-J.; Wei, S.-Y.; Huang, J.-K.; Lin, Y.-F.; Lien, C.-H.; Li, L.-J. Multilayer

graphene-WSe₂ heterostructures for WSe₂ Transistors. ACS Nano **2017**, 11 (12), 12817–12823.

- (27) Lee, J. S.; Choi, S. H.; Yun, S. J.; Kim, Y. I.; Boandoh, S.; Park, J.-H.; Shin, B. G.; Ko, H.; Lee, S. H.; Kim, Y.-M.; Lee, Y. H.; Kim, K. K.; Kim, S. M. Wafer-scale single-crystal hexagonal boron nitride film via self-collimated grain formation. *Science* **2018**, 362 (6416), 817.
- (28) Roy, T.; Tosun, M.; Kang, J. S.; Sachid, A. B.; Desai, S. B.; Hettick, M.; Hu, C. C.; Javey, A. Field-effect transistors built from all two-dimensional material components. *ACS Nano* **2014**, *8* (6), 6259–6264.
- (29) Buscema, M.; Groenendijk, D. J.; Blanter, S. I.; Steele, G. A.; van der Zant, H. S. J.; Castellanos-Gomez, A. Fast and broadband photoresponse of few-layer black phosphorus field-effect transistors. *Nano Lett.* **2014**, *14* (6), 3347–3352.